RSC Advances

RSC Publishing

PAPER

View Article Online
View Journal | View Issue

From flexible to mesoporous polybenzoxazine resins templated by poly(ethylene oxide-*b*-ε-caprolactone) copolymer through reaction induced microphase separation mechanism†

Cite this: *RSC Advances*, 2013, **3**, 6485

Wei-Cheng Chu, Jheng-Guang Li and Shiao-Wei Kuo*

When we blended the diblock copolymer poly(ethylene oxide-*b*-ε-caprolactone) (PEO-*b*-PCL) with the monomer (3-phenyl-3,4-dihydro-2*H*-1,3-benzoxazin-6-yl)methanol (PA-OH), Fourier transform infrared (FTIR) spectroscopy revealed that the ether groups of the PEO block were stronger hydrogen-bond acceptors for the OH group of PA-OH than were the C=O groups of the PCL block. Thermal curing resulted in the block copolymer being incorporated into the polybenzoxazine resin, forming cylindrical, wormlike, and disordered spherical nanostructures through a mechanism involving reaction-induced microphase separation, as evidenced using transmission electron microscopy (TEM) and small-angle X-ray scattering (SAXS). Wormlike micelles of PCL, formed as the second phase in polybenzoxazine at a high aspect ratio, appearing to possess the optimal length scale to result in greater toughness. Mild pyrolysis conditions led to removal of the PEO-*b*-PCL diblock copolymer and formation of mesoporous polybenzoxazines. This approach also provided composition-dependent nanostructures that were similar to the structures of the non-pyrolyzed samples. Regular mesoporous polybenzoxazine resin was formed only when the polybenzoxazine content was 40–70 wt%. Intriguingly, the structures were affected not only by the balance between the contents of the polybenzoxazine and the diblock copolymer but also by the curing temperature and process.

Received 21st December 2012,
Accepted 19th February 2013

DOI: 10.1039/c3ra23447a

www.rsc.org/advances

Introduction

Polybenzoxazines comprise a new class of thermosetting polymers that possess intriguing properties of high thermal stability, ready processability, low water absorption, near-zero shrinkage upon curing, good mechanical integrity, and low surface energy.[1,2] One shortcoming of these resins, however, is that they are highly brittle—especially so in the case of basic bisphenol A-aniline-type (BA-a) polybenzoxazines.[3] Many attempts have been made to improve the toughness of polybenzoxazines; they generally follow two different approaches.[3] The first is the positioning of soft segments (*e.g.*, aliphatic or siloxane moieties) into the main or side chain of the polybenzoxazine resin;[3,4] this method is relatively complex, requires costly starting materials, and is limited to the laboratory scale when it requires the synthesis of new benzoxazine materials. The second approach involves blending with other polymers[5] or nanofillers[6] as toughness agents [*e.g.*, polyurethane, liquid rubber, poly(caprolactone) (PCL), and polysiloxanes], which can be prepared on large scales, using simple methods and cheap starting materials, to provide systems that possess mechanical flexibility. Unfortunately, such blended homopolymers usually undergo macrophase separation within the polybenzoxazines as a result of a so-called ''reaction-induced phase separation'' mechanism.[7]

Recently, many attempts to improve the toughness of brittle epoxy resins have involved the use of self-assembled amphiphilic block copolymers to form a variety of ordered or disordered nanostructures in thermoset blends.[8,9] These amphiphilic block copolymers usually contain ''epoxy-miscible'' and ''epoxy-immiscible'' block segments; poly(ethylene oxide) (PEO) and PCL have been the miscible blocks used most widely to obtain nanostructures in epoxy thermosets.[9] Intermolecular hydrogen bonding interactions with the epoxy matrix are usually responsible for the improved miscibility and, therefore, the inhibition of macrophase separation. Similarly, such self-assembly of amphiphilic block copolymers into different thermoset polymers, including phenolic resins, have also been studied.[10] These long-range-ordered nanostructures can be formed after mixing uncured phenolic resins with block copolymers featuring a block that forms sufficiently strong hydrogen bonds with the phenolic OH groups, such

Department of Materials and Optoelectronic Science, National Sun Yat-Sen University, Kaohsiung, 804, Taiwan. E-mail: kuosw@faculty.nsysu.edu.tw

† Electronic supplementary information (ESI) available. See DOI: 10.1039/c3ra23447a

that curing of the phenolic resin will preserve the self-assembled structure without it undergoing macroscopic phase separation.[11] As a result, varying the intermolecular interactions of polybenzoxazines with block copolymer templates, such that they form sufficiently strong hydrogen bonds, appears to be a potential route toward the preparation of ordered nanostructures exhibiting enhanced toughness.

Mesoporous materials featuring controlled pore sizes are attractive to the academic and industrial communities because of their various applications in the fields of filtration, separation, sensing, catalysis, and controlled drug release.[12] The self-assembly of amphiphilic block copolymers as templates has been applied extensively for structure-directed syntheses of many mesoporous materials.[13] By taking advantage of the molecular design flexibility of polybenzoxazines and using appropriate preparation methods, we suspected that we could obtain mesoporous polybenzoxazines possessing various pore structures and sizes for various potential applications.[1a] Chang *et al.* were the first to develop nanoporous materials from bisphenol A and an amine-based polybenzoxazine (BA-a) with PCL as the labile component; they used (3-phenyl-3,4-dihydro-2*H*-1,3-benzoxazin-6-yl)methanol (PA-OH) as the end group to prepare PCLs of various molecular weights and to control the dispersion of PCL, as a microphase-separated labile constituent, within a stable polybenzoxazine matrix.[14] Unfortunately, they formed only short-range-ordered nanoporous structures after eliminating the PCL through $NaHCO_3$-mediated hydrolysis. Zheng *et al.* reported a nanostructured polybenzoxazine after blending with the diblock copolymer poly(styrene-*b*-*N*-vinylpyrrolidone) (PS-*b*-PVPy); this material featured only short-range-ordered and disordered nanophases—formed through a mechanism of reaction-induced microphase separation, controlled by the miscibility of the subchains of the diblock copolymer (PVPy, PS) with polybenzoxazine—before and after curing, respectively.[15] To date, the preparation of regular, ordered nanostructures and mesoporous matrices based on polybenzoxazines has remained a challenge.

The physical interactions among polybenzoxazine polymer chains—mainly through hydrogen bonding of the OH groups with the nitrogen atoms [Scheme 1(a)]—have a critical effect on the properties of these materials.[1a] These interactions are, however, a drawback when attempting to prepare polybenzoxazines that can undergo strong intermolecular hydrogen bonding with other homopolymers. Therefore, most polybenzoxazines blended with thermoplastic polymers form immiscible and phase-separated systems (*e.g.*, for PEO or PCL),[7] except when strong intermolecular hydrogen bonding is possible (*e.g.*, for PVPy).[16]

To overcome the strong intramolecular hydrogen bonding of the OH groups with the nitrogen atoms in polybenzoxazines, one approach might be to incorporate another (free)

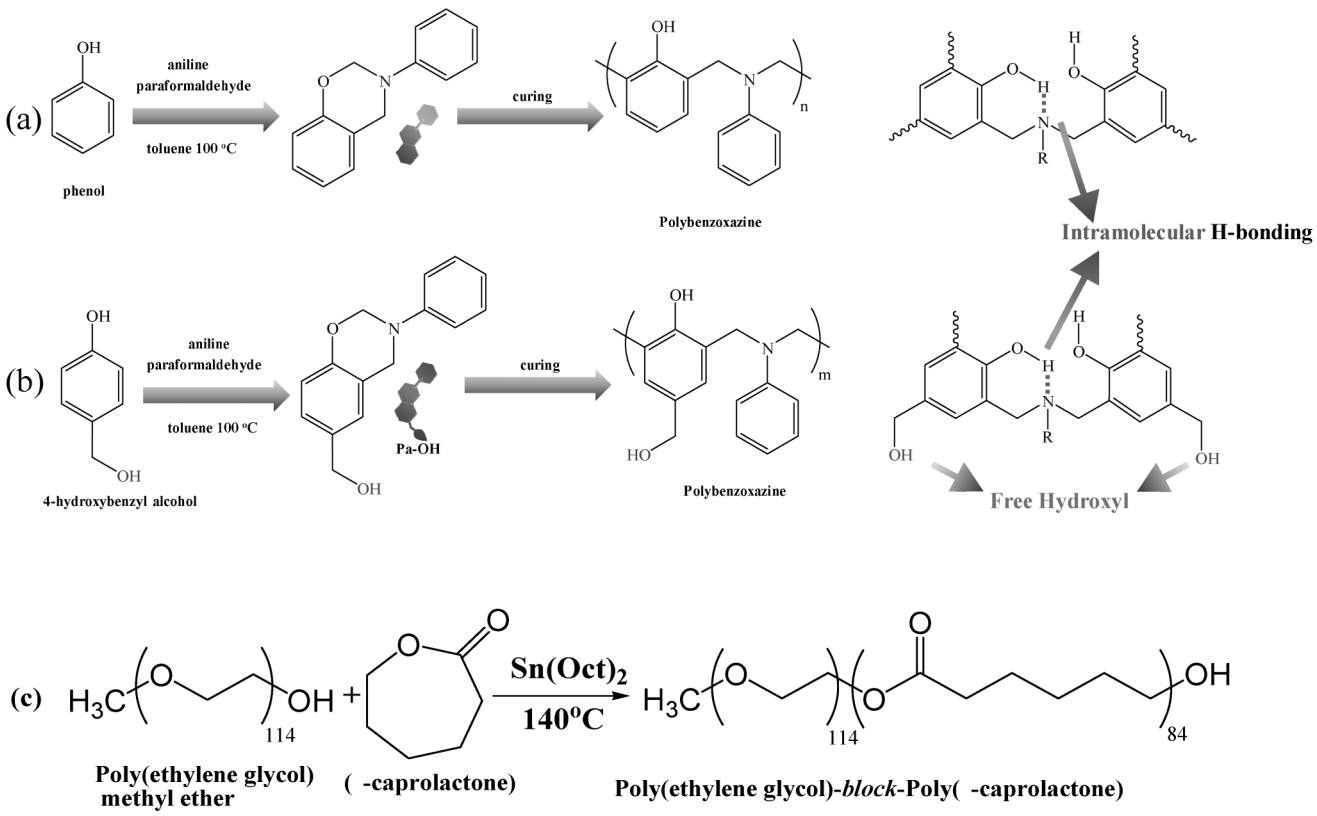

Scheme 1 (a, b) Chemical reactions and corresponding crosslinked structures of (a) PA- and (b) PA-OH-type polybenzoxazines. (c) Synthesis of PEO-*b*-PCL.

OH group into the matrix for blending with the strongly hydrogen bond–accepting block copolymers. In addition, a possible means of obtaining flexible or regular mesoporous polybenzoxazines after pyrolysis might be to use a diblock copolymer template possessing much lower glass transition and degradation temperatures, such as PEO-*b*-PCL (T_g = −60 °C for both PEO and PCL segments; T_d = 330 °C for the diblock copolymer).[10i–k] In this study, we prepared regular, ordered nanostructures, and mesoporous polybenzoxazines through blending of the monomer PA-OH—prepared from 4-hydroxybenzyl alcohol, aniline, and paraformaldehyde [Scheme 1(b)][14,17]—with the diblock copolymer PEO-*b*-PCL. We used differential scanning calorimetry (DSC), Fourier transform infrared (FTIR) spectroscopy, wide-angle X-ray diffraction (WAXD), small-angle X-ray scattering (SAXS), transmission electron microscopy (TEM), and N_2 sorption isotherms to investigate the phase behavior and competing interactions between the PA-OH-type polybenzoxazine and the diblock copolymer PEO-*b*-PCL in the mesostructures. This paper reports the first example of the preparation of flexible to mesoporous polybenzoxazine resins through competitive hydrogen bonding where the intermolecular hydrogen bonding between the PA-OH and PEO segments is stronger than that between the PA-OH and PCL segments in the blend system.

Experiments

Materials

Monomethoxy-poly(ethylene glycol) having a molecular weight of 5000 (MPEG-5 K) was obtained from Fluka and dried through azeotropic distillation with dry toluene. ε-Caprolactone (ε-CL, Acros) was purified through vacuum distillation over CaH_2; the distillation fraction collected at 96–98 °C (5 mm-Hg) was used in all polymerization reactions. Stannous(II) octoate [$Sn(Oct)_2$, Sigma] was used as received. Methylene chloride was dried over CaH_2 prior to use. Paraformaldehyde, aniline, and 4-hydroxybenzyl alcohol were purchased from Aldrich. PA-OH was obtained using a previously reported procedure [Scheme 1(b)].[14,17] The diblock copolymer PEO-*b*-PCL (M_n = 15,000; PDI = 1.28) was prepared through ring opening polymerization of ε-CL in the presence of MPEG-5 K and $Sn(Oct)_2$ [Scheme 1(c)]; its ^{1}H NMR spectrum is presented in Fig. S1, ESI.†[10k]

PA-OH

4-Hydroxybenzyl alcohol (4.96 g, 40.0 mmol) and paraformaldehyde (2.40 g, 80.0 mmol) were placed in a 100-mL three-neck flask cooled in an ice bath and then a solution of aniline (3.72 g, 40.0 mmol) in toluene (60 mL) was added. The mixture was heated under reflux at 100 °C for 8 h. After cooling to room temperature, the solid residue was filtered off and recrystallized (toluene) to afford pale-yellow crystals (80%). ^{1}H NMR ($CDCl_3$, ppm): 4.55 (s, $ArCH_2OH$), 4.63 (s, CCH_2N), 5.36 (s, NCH_2O), 6.77–7.40 (m, Ar). ^{13}C NMR ($CDCl_3$, ppm): 50.48 (CCH_2N), 64.86 ($ArCH_2OH$), 79.45 (NCH_2O). IR (KBr, cm^{-1}): 3350 (OH stretching), 947 (out-of-plane CH bending).

Nanostructured and mesoporous polybenzoxazines

PA-OH and PEO-*b*-PCL were dissolved in THF at different ratios until the solutions were homogenous. The solvent was evaporated slowly at room temperature and then the samples were vacuum-dried at 30 °C overnight. Curing of the samples was performed using the following temperature profile: 110 °C for 3 h, 150 °C for 2 h, 180 °C for 2 h, 200 °C for 2 h, 220 °C for 1 h, and 240 °C for 0.5 h. Pyrolysis of the crosslinked samples was performed by slowly heating from room temperature to 330 °C at a heating rate of 1 °C min^{-1} without a protective gas atmosphere.

Characterization

DSC was performed using a TA-Q20 instrument operated at a scan rate of 20 °C min^{-1} over a temperature range from 0 to 250 °C under a N_2 atmosphere. For non-isothermal crystallization experiments, the samples were first annealed at 250 °C for 10 min and then crystallization exotherms were recorded while cooling the sample to −90 °C at 5 °C min^{-1}. The thermal stabilities of the samples were characterized using a TA Q-50 thermogravimetric analyzer operated under a N_2 atmosphere. The cured sample (*ca.* 7 mg) was placed in a Pt cell and heated at a rate of 20 °C min^{-1} from 30 to 800 °C under a N_2 flow rate of 60 mL min^{-1}. FTIR spectra of the samples were recorded using the conventional KBr disk method and a Bruker Tensor 27 FTIR spectrophotometer.

SAXS was performed using a Nanostar U small-angle X-ray scattering system (Bruker, Germany) and Cu-Kα radiation (40 kV, 35 mA). The *d* spacings were calculated using the formula $d = 2\pi/q$. WAXD data were collected using the BL17A1 wiggler beamline of the National Synchrotron Radiation Research Center (NSRRC), Taiwan. A triangular bent Si (111) single crystal was employed to obtain a monochromated beam having a wavelength (λ) of 1.33001 Å. Nitrogen sorption isotherms were measured at 77 K using an ASAP 2020 analyzer. Prior to measurement, the samples were degassed under vacuum at 200 °C for at least 6 h. The Brunauer–Emmett–Teller (BET) method was used to calculate the specific surface areas. Using the Broekoff–de Boer (BdB) sphere model, the pore volumes and pore size distributions were derived from the adsorption branches of the isotherms; total pore volumes were estimated from the adsorbed amount at a relative pressure (P/P_0) of 0.995. The calibration curve was obtained using silica-alumina (part no. 004-16821-00) as a reference material and N_2 as the adsorption gas. TEM was conducted using a JEOL 3010 microscope (Japan) operated at 200 kV. Ultrathin sections of the samples were prepared using a Leica Ultracut S microtome equipped with a diamond knife; slices (thickness: *ca.* 700 Å) were cut at room temperature. The ultrathin sections were placed onto Cu grids coated with carbon supporting films and then stained through exposure to the vapor from 4% aqueous RuO_4 for 25 min. The mesoporous polybenzoxazines obtained after pyrolysis were not stained because of the greater difference in electron density between the self-assembled domains after selective degradation of the diblock copolymer.

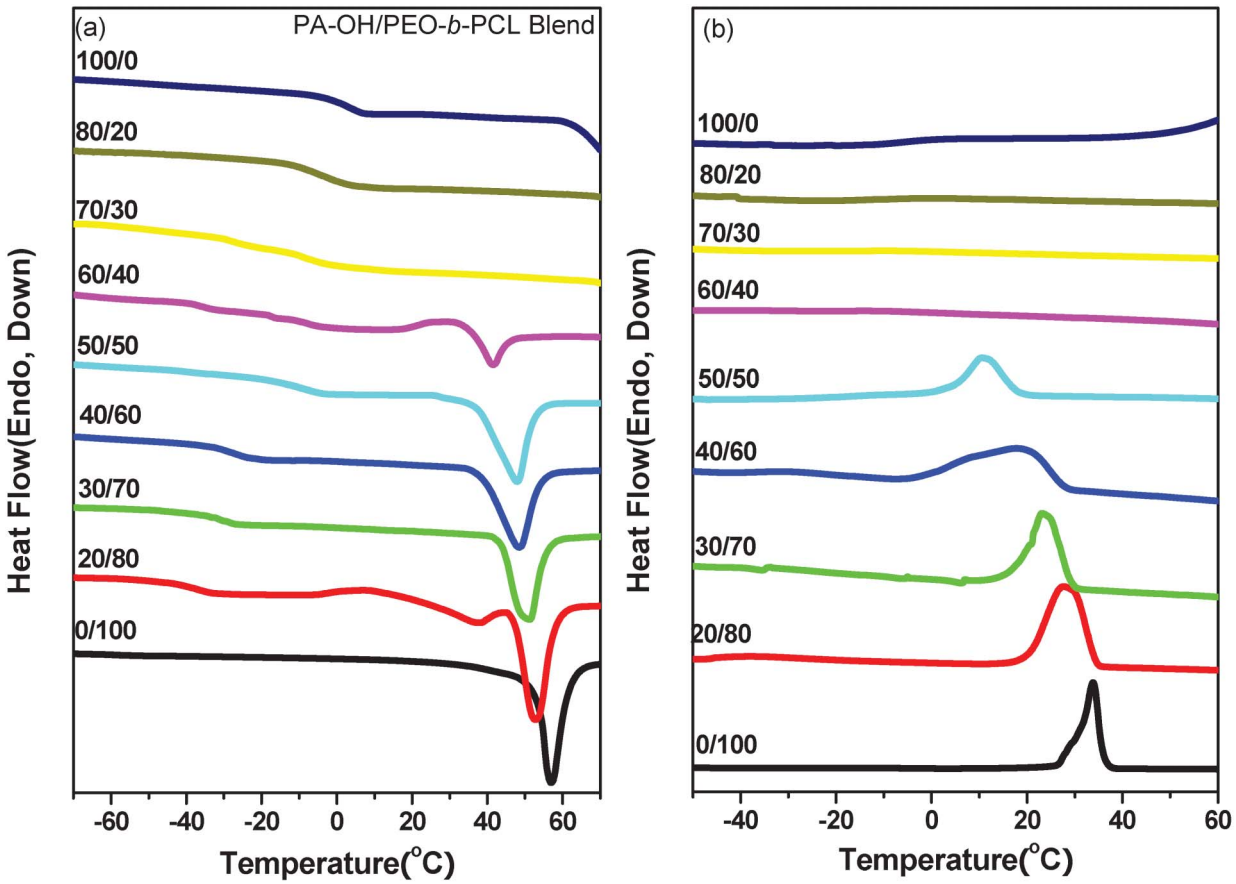

Fig. 1 DSC thermograms of PA-OH/PEO-*b*-PCL blends of various compositions: (a) second run; heating rate: 20 °C min^{-1}; (b) first run; cooling rate: 5 °C min^{-1}.

Results and discussion

Analyses of PA-OH/PEO-*b*-PCL block copolymer blends

DSC is a convenient method for determining the miscibility of polymer blends. Fig. 1 displays the conventional second-heating runs (recorded at a heating rate of 20 °C min^{-1}) and first cooling runs (cooling rate: of 5 °C min^{-1}) in the DSC thermograms of PA-OH/PEO-*b*-PCL blends of various compositions. PA-OH exhibited a melting temperature near 90 °C (Fig. S2, ESI†), similar to those of other benzoxazine monomers,[1a] as well as a glass transition temperature (T_g) near 4 °C. Low-molecular-weight compounds presenting OH groups typically feature a single glass transition during their second heating scans.[18] Because the values of T_g of PEO and PCL are very similar (T_g = −60 °C), the miscibility between PEO and PCL cannot be determined from the number of glass transitions. Guo *et al.* reported that two separate crystalline microdomains exist in diblock copolymers comprising PEO and PCL blocks.[19] The glass transitions of the PEO and PCL blocks shifted toward higher temperatures when 20–70 wt% PA-OH was present. The changes in the values of T_g arose from the existence of PA-OH/PEO (higher T_g) and the PA-OH/PCL (lower T_g) phases because the inter-association equilibrium constant between the OH group and the PEO ether oxygen atoms was greater than the inter-association equilibrium constant between the OH group and the C=O groups of PCL.[20a] The PA-OH/PEO-*b*-PCL blends exhibited only one value of T_g when the PA-OH content was greater than 80 wt%, suggesting that these blends became miscible. In addition, the melting [Fig. 1(a)] and crystallization [Fig. 1(b)] temperatures of the PEO and PCL blocks both decreased upon increasing the PA-OH content, presumably because of the morphological effects and thermodynamic consequences of the hydrogen bonding interactions.[20] Table 1 summarizes the thermal properties of PA-OH/PEO-*b*-PCL blends determined from our DSC analyses. Clearly, when the PA-OH content was less than 70 wt%, phase separation occurred; at 80 wt%, however, PA-OH acted as a common solvent for PEO and PCL, inducing the blends to

Table 1 Thermal properties of PA-OH/PEO-*b*-PCL blends

PA-OH/PEO-*b*-PCL	T_f (°C)	T_m (°C)	T_g (°C)
0/100	33.1	56.6	−60
20/80	27.8	51.6/35.8	−52.6/−38.1
30/60	22.8	50.2	−48.5/−33.2
40/60	19.3	48.0	−42.2/−26.8
50/50	11.1	47.6	−38.6/−12.9
60/40	—	40.7	−35.4/−11.1
70/30	—	—	−26.8/−6.1
80/20	—	—	−4.3

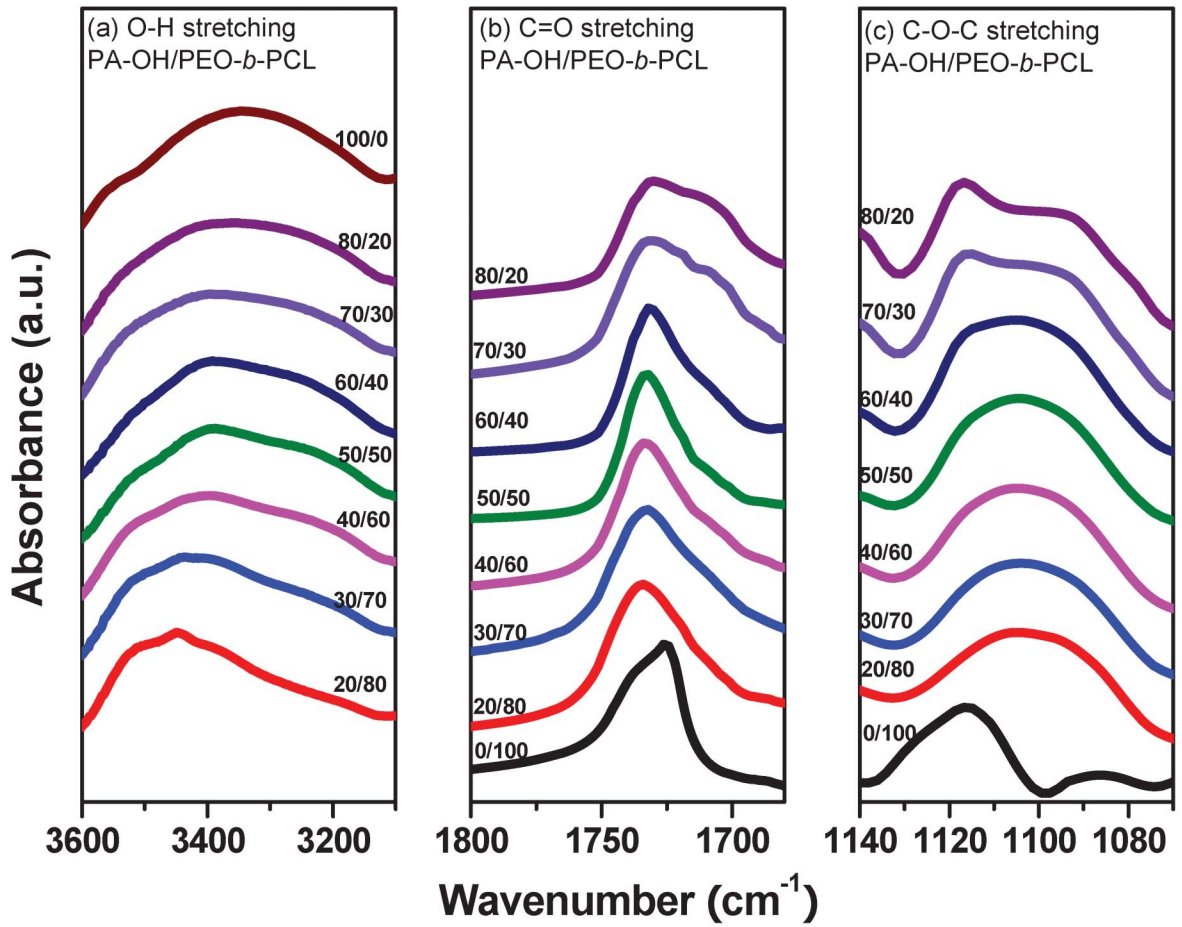

Fig. 2 Room-temperature FTIR spectra of PA-OH/PEO-*b*-PCL blends, displaying the (a) OH stretching, (b) C=O, and (c) ether regions.

become totally miscible (disordered structure). This behavior is similar to that of many ternary blends[21] that become totally miscible when the content of a polymer presenting OH groups is greater than 65 wt%.

Next, we used FTIR spectroscopy to provide evidence for hydrogen bonding within the PA-OH/PEO-*b*-PCL matrix. The signals in the OH stretching region of the room-temperature FTIR spectra of the blends of the diblock copolymer PEO-*b*-PCL and PA-OH, cast from THF solutions, were sensitive to the presence of hydrogen bonds [Fig. 2(a)]. The spectrum of PA-OH featured two major unresolved bands in the OH stretching region, corresponding to the free OH groups at 3525 cm^{-1} and a broad band centered at 3400 cm^{-1} arising from absorption of hydrogen-bonded OH groups (self-association). The intensity of the signal for the free OH groups decreased gradually upon increasing the content of the diblock copolymer PEO-*b*-PCL, as we had expected. The broad band of pure PA-OH at 3400 cm^{-1} became even broader when it was blended with PEO-*b*-PCL at higher PA-OH content, indicating that the OH group of PA-OH interacted with both the ether groups of PEO and the C=O groups of PCL. We assign the signals at lower and higher wavenumbers to the OH groups involved in OH···ether and OH···O=C interactions, respectively, because the average hydrogen bonding strength follows the order OH···ether > OH···OH > OH···O=C.[20a]

The C=O groups of PCL blocks are also sensitive to hydrogen bonding interactions. The signal for C=O stretching of pure PCL [Fig. 2(b)] is split into two bands representing amorphous and crystalline conformations at 1734 and 1724 cm^{-1}, respectively.[22] We assign another contribution near 1705 cm^{-1} to the C=O groups of PCL that were hydrogen bonded to the OH groups of PA-OH. The signal for the hydrogen-bonded C=O groups of PCL appeared in the spectra of the blends containing a PA-OH content of 70 wt% or greater, indicating that the OH groups of PA-OH began to interact with the C=O groups of PCL at a PA-OH content of 70 wt%. As expected, a higher content of OH units resulted in a higher number of hydrogen-bonded C=O groups. A band at 1100 cm^{-1} also characterized the hydrogen-bonding interactions between the OH group of PA-OH and the ether oxygen atoms of PEO. Fig. 2(c) presents scale-expanded FTIR spectra in the range 1050–1140 cm^{-1} for various PA-OH/PEO-*b*-PCL blends. Pure PEO-*b*-PCL features a characteristic band at 1116 cm^{-1} that corresponds to the C–O–C ether unit of the PEO block. Upon formation of hydrogen bonds between PA-OH and the ether oxygen atoms of PEO, at a PA-OH content of 20 wt% or greater, this band shifted to 1102 cm^{-1}.[10j]

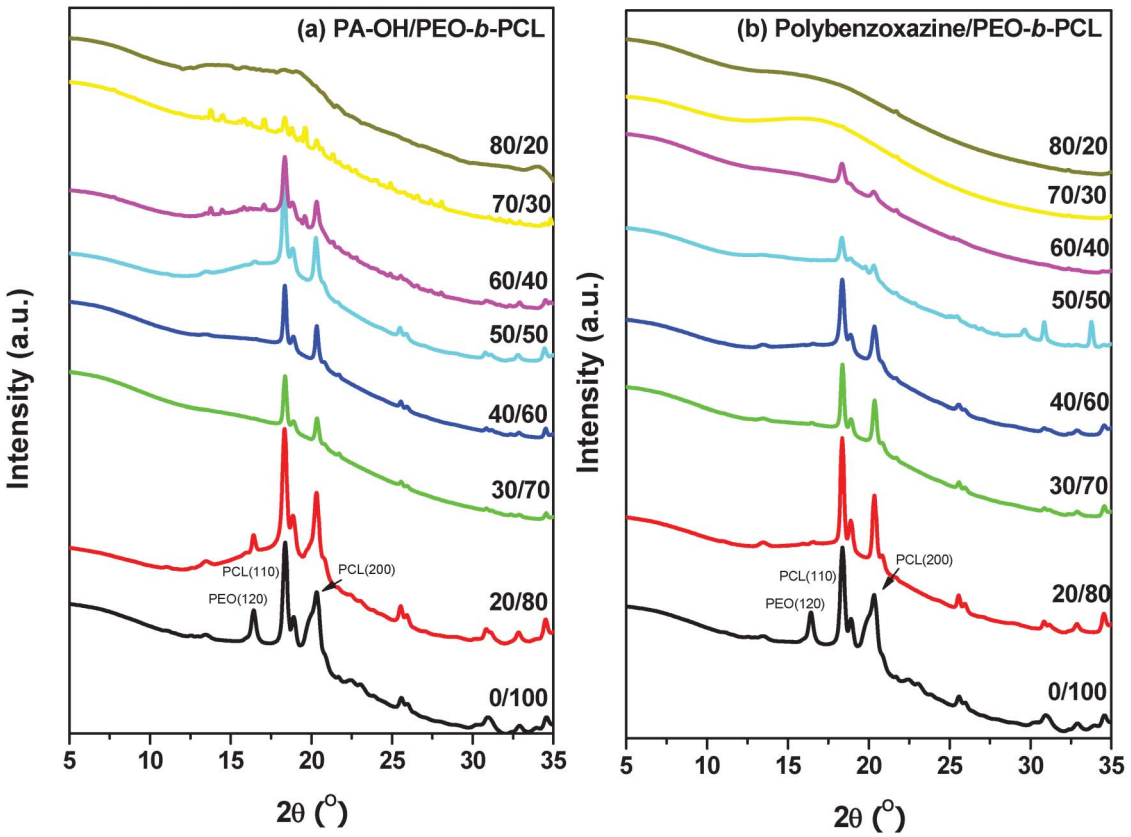

Fig. 3 Room-temperature WAXD patterns of (a) PA-OH/PEO-*b*-PCL and (b) polybenzoxazine/PEO-*b*-PCL blends of various compositions.

Fig. 3(a) displays WAXD data of PA-OH/PEO-*b*-PCL blends of various compositions at room temperature. The crystalline PEO exhibited one peak at a value of 2θ of 16.5°, representing the (120) reflection;[23] the crystalline PCL provided two distinct diffraction peaks for all blends at values of 2θ of 18.3 and 20.3°, representing (110) and (200) reflections of the orthorhombic packing that is the preferred crystallographic orientation of pure PCL.[24] Notably, the crystallization peaks remained almost identical at a PA-OH content of 20 wt%, indicating that crystalline PEO and PCL both remained. This result is consistent with the two melting points observed through DSC analyses, where the lower and higher values corresponded to crystalline PEO and crystalline PCL, respectively. Interestingly, the crystallization peak of PEO disappeared after blending at a PA-OH content greater than 30 wt%, whereas the crystallization peaks of PCL remained when the PA-OH content in the blend was less than 60 wt%; therefore, we observed only a single melting temperature (corresponding to crystalline PCL) when the PA-OH content was less than 60 wt% in the DSC analyses in Fig. 1(a). The crystallization peaks of both PEO and PCL disappeared when the PA-OH content was greater than 70 wt%, consistent with the C=O groups of PCL already interacting with the OH group of PA-OH, based on FTIR spectroscopic analysis [Fig. 2(b)], and the melting peak having disappeared, based on DSC analyses [Fig. 1(a)]. From the DSC, FTIR spectroscopic, and WAXD analyses, we conclude that the OH groups of PA-OH interacted completely with the ether oxygen atoms of the PEO block at relatively lower PA-OH contents and then interacted with the C=O groups of the PCL block at relatively higher PA-OH contents (>70 wt%) to form miscible disorder structures.

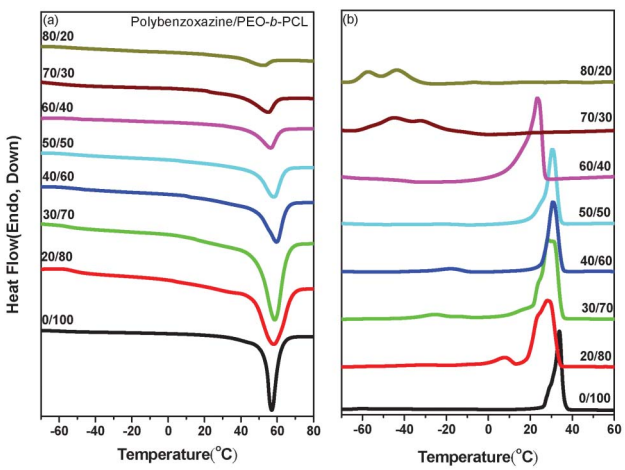

Fig. 4 DSC thermograms of polybenzoxazine/PEO-*b*-PCL blends of various compositions: (a) second run; heating rate: 20 °C min^{-1}; (b) first run; cooling rate: 5 °C min^{-1}.

Analyses of polybenzoxazine/PEO-*b*-PCL block copolymer blends

We incorporated the diblock copolymer PEO-*b*-PCL into polybenzoxazine to prepare nanostructures. Prior to thermal curing, all of our binary mixtures of the benzoxazine PA-OH and the diblock copolymer PEO-*b*-PCL were homogenous and transparent. After thermal curing, the polybenzoxazines remained homogenous and transparent, but became dark red in color, suggesting that macrophase separation had not occurred. Nevertheless, we could not explain reaction-induced microphase separation merely in terms of sample clarity. Fig. 4 displays the conventional second-heating runs, recorded at a heating rate of 20 °C min^{-1}, and first cooling runs, recorded at a cooling rate of 5 °C min^{-1}, in the DSC thermograms of polybenzoxazine/PEO-*b*-PCL blends of various compositions after curing. Clearly, all of the blends exhibited the melting temperature that corresponded to crystalline PCL. The amorphous phase of PCL in the PA-OH/PEO-*b*-PCL blends at PA-OH contents greater than 70 wt% become a crystalline phase after the curing of PA-OH, due to a ''reaction-induced phase separation'' mechanism.[25]

Similarly, the signal for the hydrogen-bonded C=O groups of PCL in the FTIR spectrum at 1705 cm^{-1} disappeared when the content of the PA-OH–type polybenzoxazine was greater than 70 wt% after thermal curing; only a signal for the crystalline peak was present near 1724 cm^{-1} for all of the blend systems [Fig. 5(b)]. In addition, the ether oxygen atoms of PEO remained hydrogen bonded to the PA-OH-type polybenzoxazine after thermal curing of all of the blends, as evidenced by the C–O–C band also shifting to 1102 cm^{-1}. Fig. 3(b) presents the WAXD data of the polybenzoxazine/PEO-*b*-PCL blends of various compositions at room temperature. The PEO crystallization peak disappeared after thermal curing to form the blended polybenzoxazine at all compositions, but the crystallization peaks of PCL remained when the PA-OH content in the blend was less than 60 wt%; as a result, only a single melting point (corresponding to crystalline PCL) appeared at all compositions. Further increasing the polybenzoxazine content to 70–80 wt% caused the PCL crystallization peak to disappear and resulted in amorphous halos in the WAXD pattern, indicating that the crystalline structure of the PCL block had been destroyed. This result is, however, in contrast to the DSC data in Fig. 4(a), which reveals that the polybenzoxazine/PEO-*b*-PCL = 70/30 and 80/20 blends both exhibited the strong melting peaks of the crystalline PCL. In general, polymer crystallinity measured through WAXD arises from *in situ* measurement with no thermal history involved in preparing the sample. In contrast, polymer crystallinity detected through DSC is dependent on the thermal history, because recrystallization may occur during the cooling or heating scan. According to our DSC data [Fig. 4(b)], we find that the polybenzoxazine/PEO-*b*-PCL = 70/30 and 80/20 blends required certain degrees of supercooling to initiate crystallization of their PCL blocks. It is well-established that freezing temperature (T_f)—associated nonisothermal crystallization displays a distinct correlation with the microdomain structure. For example, the value of T_f was found to drop abruptly as the melt morphology changed from extended lamellae to dispersed cylinders; a second decrease in the freezing temperature has been observed when the morphology underwent a further transformation into spheres. The degree of supercooling ($\Delta T = T_m^0 - T_c$, T_m^0 = 75 °C)[26] required to initiate crystallization in the lamellar microdomains (ΔT = 50 °C) is comparable with that associated with the PCL homopolymer (ΔT = 42 °C); exceedingly large undercoolings are required for crystallizations in cylindrical microdomains (ΔT = 125 °C).[26f] For example, polybenzoxazine/PEO-*b*-PCL = 70/30 (at *ca.* −31 and −45 °C) and 80/20 (at *ca.* −43 and −57 °C) displays two freezing temperatures. Crystallization may occur with more than one exotherm—a phenomenon that is termed ''fractionated crystallization'' by different shapes of nanodomains.[27] As a result, these samples required cooling down to temperatures below −50 °C to initiate crystallization of the PCL block, as we have described previously.[27c–e]

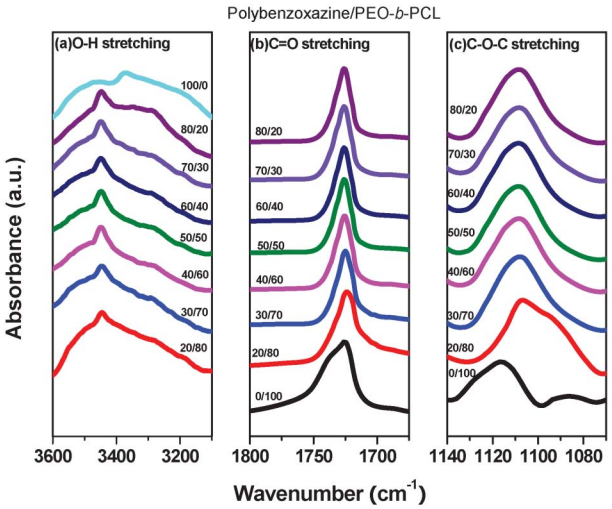

Fig. 5 Room-temperature FTIR spectra of polybenzoxazine/PEO-*b*-PCL blends, displaying the (a) OH stretching, (b) C=O, and (c) ether regions.

We recorded SAXS profiles of the polybenzoxazine resins templated by the block copolymer PEO-*b*-PCL at room temperature to confirm the self-organized morphologies. Fig. 6(a) displays SAXS profiles of the polybenzoxazine/PEO-*b*-PCL blends at room temperature. The pure PEO-*b*-PCL block copolymer exhibited lamellar character, as determined by the special ratio of q^* and $2q^*$.[10i] At polybenzoxazine contents of less than 50 wt%, we observed only one broad peak, which corresponded to long periods of crystalline PCL (*ca.* 15.1 nm). Further increasing the polybenzoxazine content led to more obvious peaks, due to more-ordered structures at these compositions. For example, the profile of polybenzoxazine/PEO-*b*-PCL = 60/40 featured another small peak near $\sqrt{7}$, due to incomplete disordering of the hexagonal cylinders or wormlike structures present in this blend, and those of the polybenzoxazine/PEO-*b*-PCL = 70/30 and 80/20 blends featured structures with greater long-range order, with a ratio of peak positions of $1 : \sqrt{3}$, reflecting an ordered phase of hexagonally packed cylinders. We also recorded the SAXS profiles at 80 °C—a temperature higher than the values of T_m of both crystalline PEO and crystalline PCL [Fig. 6(b)]. The broad peaks disappeared and no scattering peaks

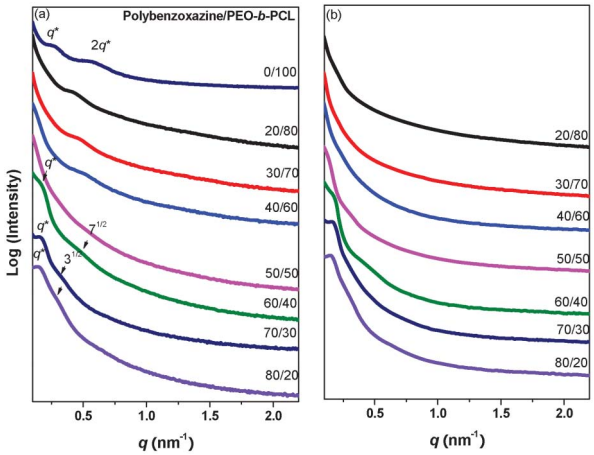

Fig. 6 SAXS profiles of polybenzoxazine/PEO-*b*-PCL blends at various compositions, recorded at (a) 25 and (b) 80 °C.

were present when the polybenzoxazine content was less than 40 wt%, suggesting the presence of disordered polybenzoxazine resins. This behavior is similar to that of many previously reported thermoset/block copolymer blends;[28] it suggests that insufficient polybenzoxazine resin was present relative to the templating PEO-*b*-PCL block copolymer.

Fig. 7 illustrates the different types of self-assembled morphologies observed using TEM. After RuO_4 staining, the polybenzoxazine/PEO microdomains were dark and the PCL microdomains appeared light. Clearly, wormlike and rodlike structures (partial cylinders and partial lamellae, respectively, in the blends) were visible at polybenzoxazine contents of 40 and 50 wt% [Fig. 7(a) and (b)]. The long-range order of the structures improved after increasing the polybenzoxazine content to greater than 60 wt% [Fig. 7(c) and (d)], consistent with the SAXS data. This behavior suggests that wormlike to spherical (micelle) structures were formed with short-range order. Such structures are similar to those found in previous studies of phenolic/PS-*b*-P4VP = 80/20 blend[29] and polybenzoxazine/PS-*b*-PVP = 80/20 systems.[15] The formation of nanostructures in thermosets templated by amphiphilic block copolymers could occur through mechanisms involving reaction-induced microphase separation. The wormlike and spherical micelle structures both appear in Fig. 7(d), consistent with the DSC data in Fig. 4(b), suggesting that ''fractionated crystallization'' by different shapes of nanodomains occurred in this blend.

Bates and co-workers investigated the impact of different nanostructures of block copolymers on the mechanical properties of thermoset blends.[8] The toughening effect is significantly dependent on the shape and size of the second phase, as well as the interactions of the second phase within the thermoset matrix. Toughening mechanisms from wormlike micelle-modified epoxy resins have been studied previously; wormlike micelles having a high aspect ratio might present an optimal length scale, resulting in greater toughness than that of other morphologies.[8] As a result, we suspected that our present polybenzoxazine/PEO-*b*-PCL = 60/40 blend might exhibit flexibility as a result of its wormlike structure. Fig. 8 displays the phase behavior of the polybenzoxazine/PEO-*b*-PCL = 60/40 blend, as determined through dynamic mechanical analysis, as well as the storage modulus and the tan δ–temperature curves. The value of T_g of the PA-OH–type polybenzoxazine was approximately 266 °C, and the values of T_g and T_m of the PCL block segment were approximately −40 and 48 °C, respectively. Fig. 8 also displays a photograph of this blend system, revealing a dark red transparent film (dimensions: 3 cm × 1 cm × 0.1 cm) that could be bent,

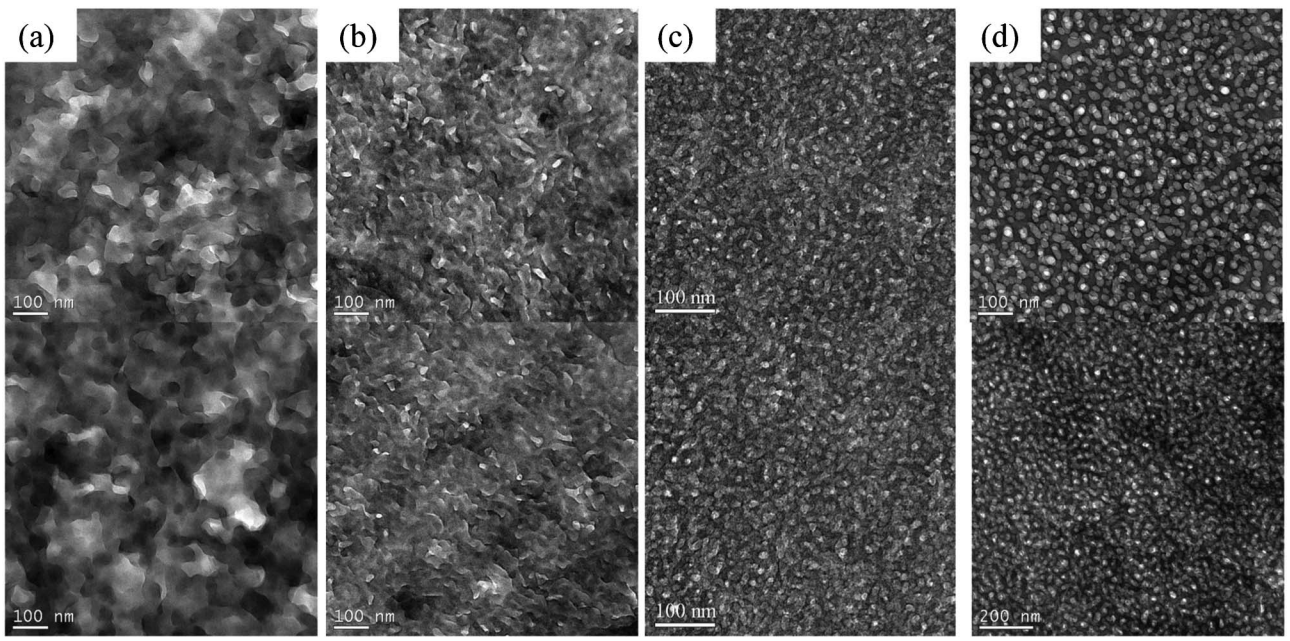

Fig. 7 TEM images of polybenzoxazine/PEO-*b*-PCL blends: (a) 40/60, (b) 50/50, (c) 60/40, and (d) 70/30.

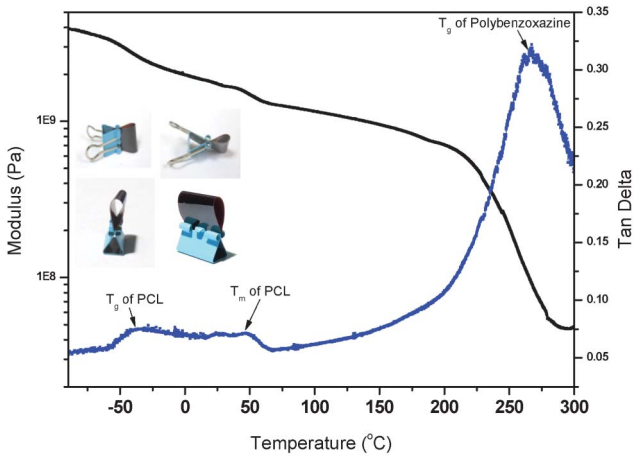

Fig. 8 Dynamic mechanical analysis of the polybenzoxazine/PEO-*b*-PCL = 60/40 blend; inset: photograph of its corresponding thin film.

suggesting significantly enhanced toughness relative to BA-a–type polybenzoxazine. As a result, forming wormlike micelles of flexible diblock copolymer segments in the surrounding polybenzoxazine matrix could be a promising approach toward obtaining high-performance with toughness properties.

Scheme 2 displays a possible mechanism for the self-assembly of nanostructures from polybenzoxazine/PEO-*b*-PCL blends. In the first step, the PA-OH precursor behaves as a common solvent for the PEO-*b*-PCL diblock copolymer to form a miscible disordered structure through hydrogen bonding prior to thermal curing [Scheme 2(a)]; as a result, we observed one value of T_g for the PA-OH/PEO-*b*-PCL blends at higher PA-OH contents [see Fig. 1(a)]. Nevertheless, microphase separation occurred at lower PA-OH contents, where intermolecular hydrogen bonding between the PA-OH and PEO units was stronger than that between the PA-OH and PCL units. During thermal curing, however, miscibility of the PA-OH–based polybenzoxazine with PEO resulted from the formation of intermolecular hydrogen bonds between the ether oxygen atoms of PEO and the free OH groups of the polybenzoxazine [Scheme 2(b)]. After thermal curing, the reaction-induced microphase separation was complete; the PEO segments were presumably miscible with the PA-OH-based polybenzoxazine, but the PCL segments were excluded from this miscible domain [Scheme 2(c)] and then formed crystalline domains, as evidenced by the DSC and FTIR spectroscopic data in Fig. 4(a) and 5(b), respectively.

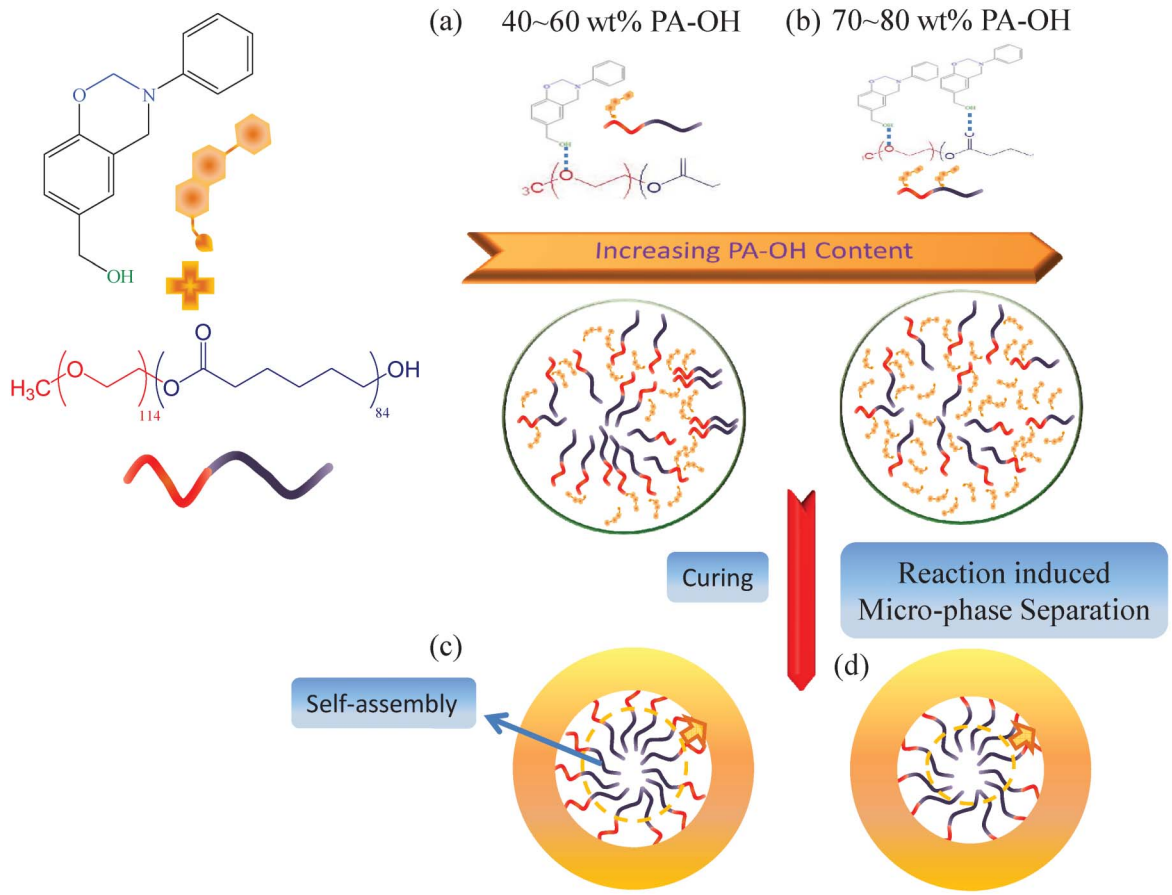

Scheme 2 (a), (b) Inter-association between PA-OH with PEO-*b*-PCL with different PA-OH content, and (c), (d) thermal curing induced microphase separation with different PA-OH type polybenzoxazine.

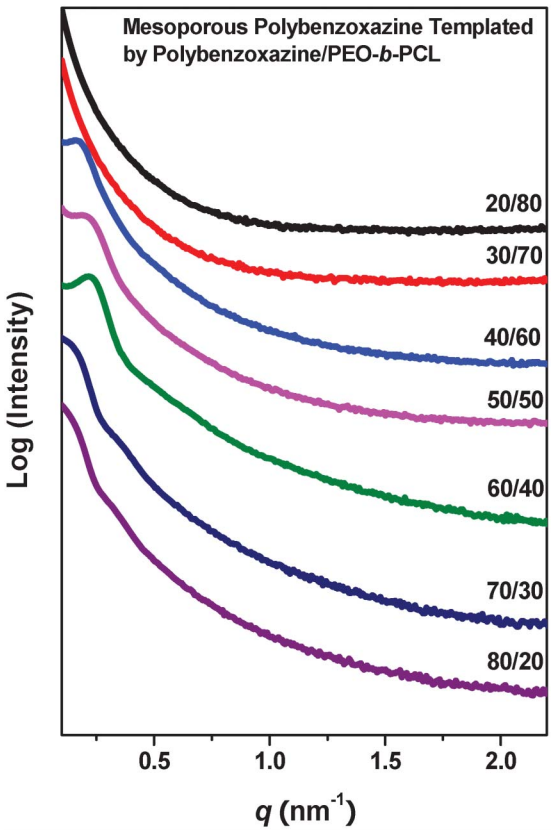

Fig. 9 Profiles of the SAXS intensities of mesoporous polybenzoxazines, templated by PEO-*b*-PCL at various compositions, after pyrolysis.

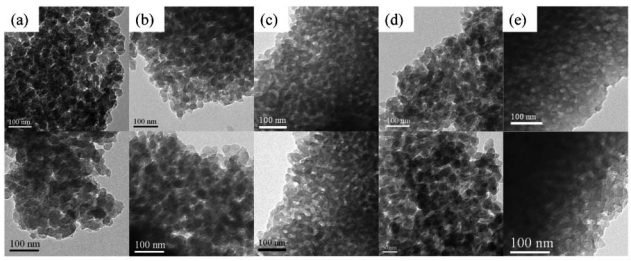

Fig. 10 TEM images of mesoporous polybenzoxazines, templated by various polybenzoxazine/PEO-*b*-PCL blends, after pyrolysis: (a) 30/70, (d) 40/60, (e) 50/50, (d) 60/40, (e) 70/30.

Analyses of mesoporous polybenzoxazine resins

For this study, we chose a temperature of 330 °C as the optimal pyrolysis temperature, because the PEO-*b*-PCL block copolymer would begin to degrade, as discussed in our previous study,[10i–k] but the weight of the cured polybenzoxazine matrix would not have decreased significantly (Fig. S3, ESI†). The TGA measurements revealed that the pure PA-OH-type polybenzoxazine underwent more than one degradation step during its thermal degradation: an initial weight loss began near 400 °C, due to the evaporation of amines, with the main degradation occurring between 500 and 600 °C, due to degradation of the phenolic moieties.[1a] Fig. 9 displays SAXS curves of the polybenzoxazine/PEO-*b*-PCL blends after pyrolysis. The scatter intensity was higher for the pyrolyzed samples than it was for the non-pyrolyzed samples, due to the increased difference in electron density between the self-assembled domains after selective degradation through pyrolysis. At lower polybenzoxazine contents (<40 wt%), the system contained insufficient polybenzoxazine resin to template the PEO-*b*-PCL block copolymer to form a disordered structure, similar to the behavior of the non-pyrolyzed samples. At polybenzoxazine content greater than 40 wt%, the scattering peaks become obvious and corresponded to those of the wormlike or rodlike mesoporous structures; that is, they did not vary significantly after pyrolysis. The first scattering peaks shifted, however, to a higher value of q, indicating decreased local variations in periodicity when the chemical bonds were broken to shrink the polybenzoxazine matrix. For example, the first peak position near 0.17 (d = 36.9 nm) for the non-pyrolyzed polybenzoxazine/PEO-*b*-PCL = 60/40 sample shifted to near 0.23 (d = 27.3 nm) for the pyrolyzed sample. In addition, the first peak position remained almost unchanged after blending with different weight percentages of the PEO-*b*-PCL block copolymer. Fig. 10 illustrates the different types of self-assembled morphologies we observed in the TEM images of the polybenzoxazine/PEO-*b*-PCL blends after pyrolysis. The mesoporous structures were similar to those of the non-pyrolyzed samples, including disordered cylinder, wormlike, and disordered spherical (micelle) morphologies. Scheme 3 summarizes the whole mechanism of mesoporous polybenzoxazine formation templated by the PEO-*b*-PCL copolymer.

We used the BET method to measure the surface areas and pore sizes of selected samples. Fig. 11 reveals that the N_2 sorption isotherm of the mesoporous polybenzoxazine formed from the system incorporating 30–60 wt% of the PEO-*b*-PCL diblock copolymer was a representative type-IV curve, with a sharp capillary condensation step for relative pressures in the range from 0.85 to 0.95. The mesoporous polybenzoxazine samples templated by PEO-*b*-PCL at polybenzoxazine contents of 40, 50, and 60 wt% exhibited typical H_1-like hysteresis loops at values of P/P_0 in the range 0.4–0.9, suggesting a common mesoporous structure having large, branched, cylindrical pores.

The H_1 hysteresis loops for these samples were characteristic of cylindrical mesopores. Based on the Harkins–Jura model,[30] the mean pore sizes measured from the adsorption branches for the mesoporous samples templated at PEO-*b*-PCL contents of 60, 50, 40, and 30 wt% were 28.4, 28.6, 16.4, and 11.5 nm, respectively. In addition, we calculated a BET surface areas of 355.3 $m^2\ g^{-1}$ for the mesoporous polybenzoxazine prepared at 60 wt% PEO-*b*-PCL, 405.5 $m^2\ g^{-1}$ for the worm-like structure prepared at 50 wt% PEO-*b*-PCL, 96.4 $m^2\ g^{-1}$ for the worm-like structure prepared at 40 wt% PEO-*b*-PCL, and only 9.0 $m^2\ g^{-1}$ for the disordered spherical (micelle) structure formed at 30 wt% PEO-*b*-PCL. Table 2 summarizes the BET surface area, pore volume, and BJH pore size of the mesoporous polybenzoxazine materials. The low surface areas of the disordered spherical (micelle) structures (templated by 30 wt% PEO-*b*-PCL) presumably resulted from the absence of

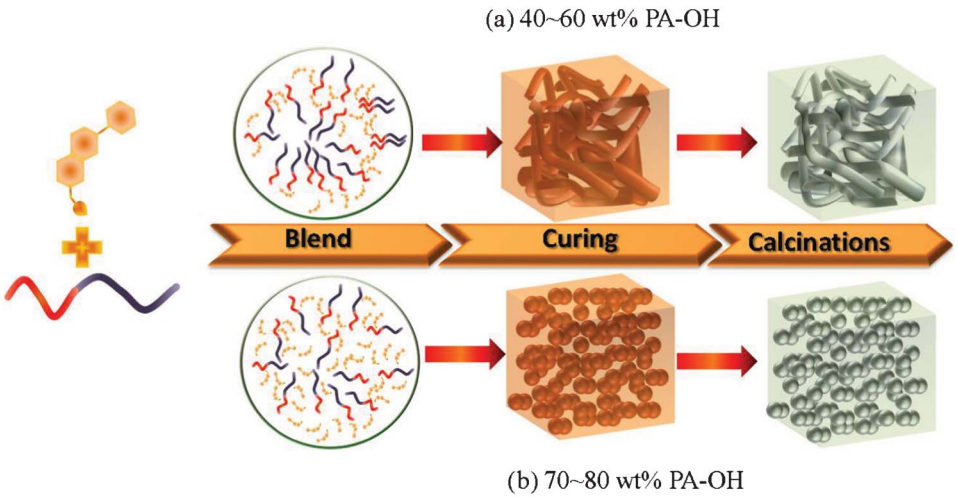

Scheme 3 Morphological changes in the self-assembled nanostructures and mesoporous polybenzoxazines with different polybenzoxazine contents.

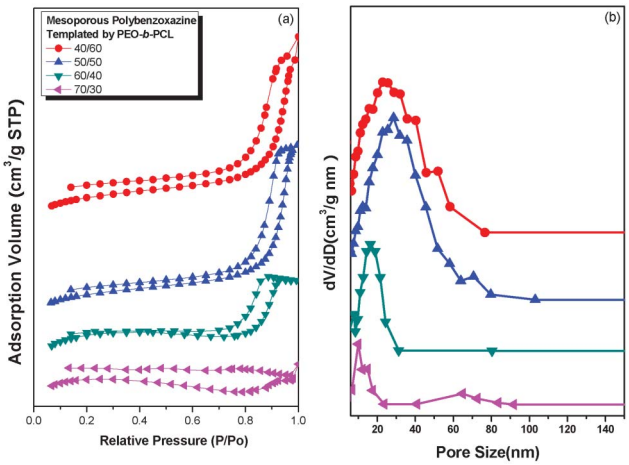

Fig. 11 (a) N_2 adsorption/desorption isotherms and (b) pore size distribution curves of mesoporous polybenzoxazine resins templated by polybenzoxazine at various weight percentages.

interconnected channels between the individual spherical domains during pyrolysis.

Because the curing temperature and process strongly affect the morphology and mechanical properties of thermoset polymers,[31] we investigated the effects of various curing temperatures and processes, as listed in Table 3, on the structures and properties of our mesoporous polybenzoxazines. Fig. 12 and 13 present SAXS data and TEM images of the pyrolyzed polybenzoxazine/PEO-*b*-PCL = 60/40 samples obtained using the various curing temperatures and processes in Table 3. The mesoporous structure was strongly dependent on the curing temperature and process. Sample (e) in Fig. 13 exhibited long-range order of its cylindrical mesoporous structure when cured at a relatively lower temperature (110 °C) of 16 h. The lower curing temperature ensured better rearrangement of the benzoxazine monomer so that it could self-assemble into the long-range-ordered structure. Fig. 14 presents the N_2 sorption isotherms of the mesoporous

Table 3 Curing temperatures and processing times of polybenzoxazine/PEO-*b*-PCL = 60/40

Samples	110 °C	150 °C	180 °C	200 °C	220 °C	240 °C
(a)	3 h	2 h	2 h	2 h	1 h	0.5 h
(b)	6 h	4 h	4 h	4 h	2 h	1 h
(c)	6 h	4 h	4 h	2 h	1 h	0.5 h
(d)	1.5 h	1 h	1 h	1 h	0.5 h	0.25 h
(e)	16 h	4 h	4 h	2 h	—	—

Table 2 Textual properties of the mesoporous polybenzoxazine resins

Polybenzoxazine/PEO-*b*-PCL	*d* (nm)[a]	Pore size (nm)	S_{BET} ($m^2\ g^{-1}$)[b]	S_M ($m^2\ g^{-1}$)[b]	Pore volume ($cm^3\ g^{-1}$)	Micropore volume ($cm^3\ g^{-1}$)
40/60	39.9	28.4	355.3	147.3	0.57	0.067
50/50	29.9	28.6	405.5	213.6	0.56	0.098
60/40	29.9	16.4	96.4	15.0	0.09	0.006
70/30	44.9	11.5	9.0	—	0.06	—
Polybenzoxazine/PEO-*b*-PCL = 60/40						
Sample a	29.9	16.4	96.4	15.0	0.09	0.006
Sample b	31.5	20.0	373.5	191.5	0.42	0.088
Sample c	31.4	20.1	276.5	104.2	0.38	0.048
Sample d	31.4	20.1	340.7	150.3	0.41	0.069
Sample e	24.4	17.7	178.5	54.2	0.32	0.024

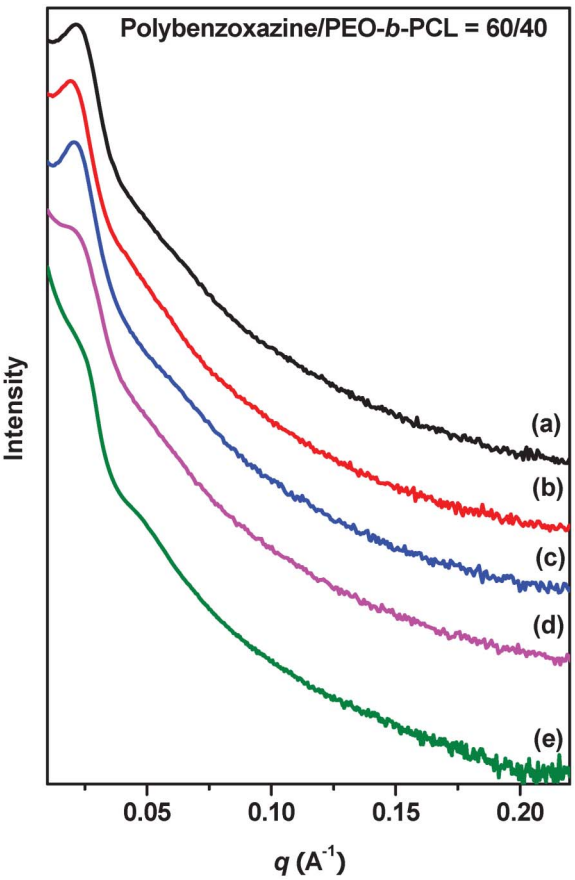

Fig. 12 SAXS profiles of mesoporous polybenzoxazines templated by polybenzoxazine/PEO-*b*-PCL = 60/40 using the curing temperatures and times listed in Table 3.

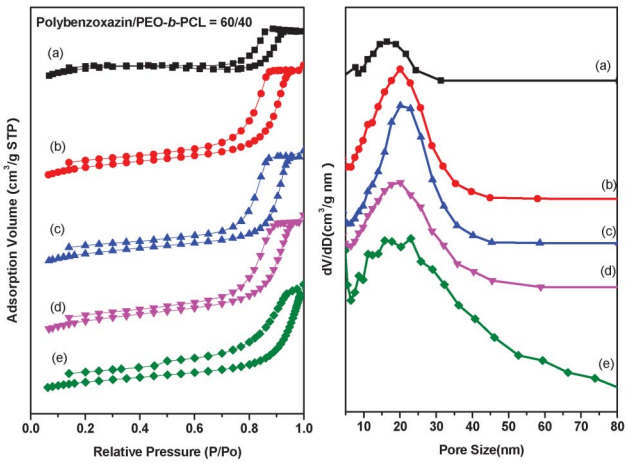

Fig. 14 (a) N_2 adsorption/desorption isotherms and (b) pore size distribution curves of mesoporous polybenzoxazine templated by polybenzoxazine/PEO-*b*-PCL = 60/40 using the curing temperatures and times listed in Table 3.

polybenzoxazines formed from the corresponding samples in Fig. 12 and 13. Again, they exhibited representative type-IV curves and H_1-like hysteresis loops, indicating a common mesoporous structure with large, branched, cylindrical pores. Table 2 also summarizes the BET surface area, pore volume, and BJH pore size of the mesoporous polybenzoxazine materials. The surface area of the mesoporous polybenzoxazines could be improved by carefully controlling the curing temperature and process. Based on SAXS, TEM, and BET analyses, the long-range order of the mesoporous structures could be improved through careful control over the curing temperature and processing conditions. In addition, the volume fractions and molecular weights of the block copolymers also strongly affected the mesoporous structure.[32] Fig. S4 and S5, ESI† display the TEM images of the mesoporous polybenzoxazines templated by various volume fractions and molecular weights of the PEO_{114}-*b*-PCL_{168} diblock copolymer and the PCL_{220}-*b*-PEO_{2272}-*b*-PCL_{220} triblock copolymer; they also possessed disordered cylinder, wormlike, or disordered

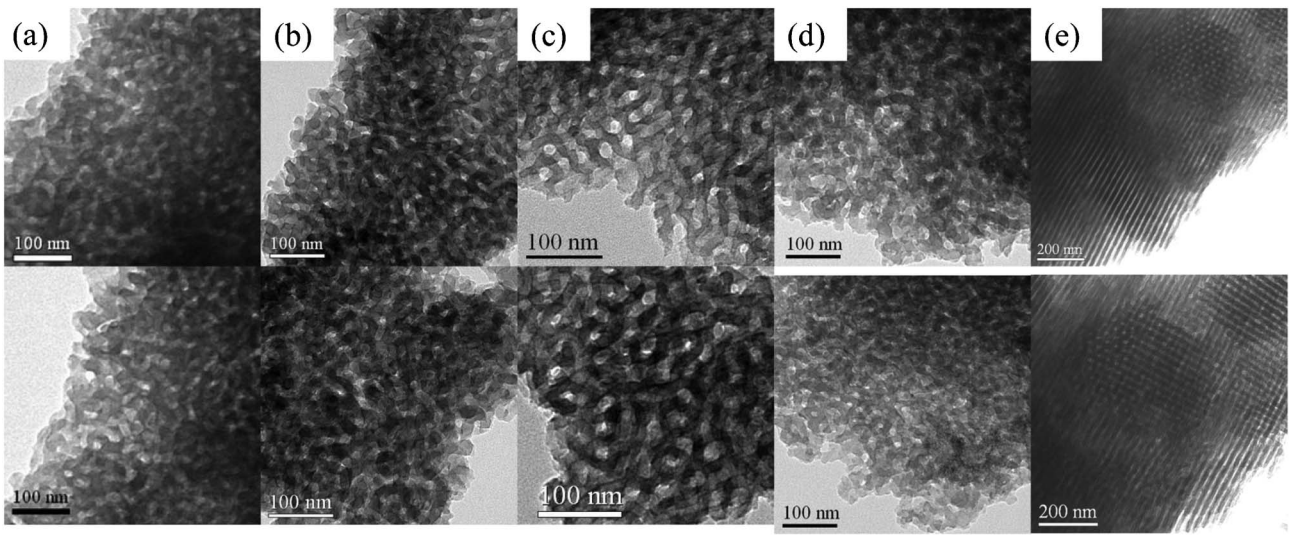

Fig. 13 TEM images of mesoporous polybenzoxazines templated by polybenzoxazine/PEO-*b*-PCL = 60/40 using the curing temperatures and times listed in Table 3.

spherical (micelle) morphologies, but with larger pore sizes than those formed using PEO_{114}-*b*-PCL_{88} as the template, due to the larger molecular weights of these two block copolymers. For example, the average pore size of the mesoporous polybenzoxazine templated by the triblock copolymer PCL_{220}-*b*-PEO_{2272}-*b*-PCL_{220} at 50 wt% was approximately 69.0 nm, as determined using the Harkins–Jura model. Again, they displayed representative type-IV curves and H_1-like hysteresis loops, indicating common mesoporous structures with large, branched, cylindrical pores (Fig. S6, ESI†). Finally, because we expect such mesoporous polybenzoxazine structures to present OH groups and have large surface areas, these materials might have potential applications as gas sensors.[12e]

Conclusions

We have employed DSC, TEM, WAXD, SAXS, and FTIR spectroscopy to investigate the miscibility, phase behavior, and hydrogen bonding within polybenzoxazine/PEO-*b*-PCL blends. DSC and FTIR spectroscopy provided evidence that the ether oxygen atoms of the PEO block were stronger hydrogen bond acceptors for the OH group of PA-OH than were the C=O groups of the PCL block. SAXS and TEM analyses indicated that polybenzoxazine/PEO-*b*-PCL blends of various compositions resulted in different microphase-separated structures, mediated through hydrogen bonding interactions. We obtained a flexible polybenzoxazine as a result of the formation of wormlike micelles of PCL, as the second phase in polybenzoxazine, with a high aspect ratio—presumably at an optimal length scale that resulted in greater toughness. Mesoporous polybenzoxazines formed after mild pyrolysis of the templating PEO-*b*-PCL diblock copolymer when the polybenzoxazine content was 40–70 wt%, through a mechanism that was affected by not only an intriguing balance between the contents of the polybenzoxazine and the diblock copolymer but also by the curing temperature and processing times.

Acknowledgements

This work was supported financially by the National Science Council, Taiwan, Republic of China, under Contract No. NSC 100-2221-E-110-029-MY3 and NSC 100-2628-E-110-001.

References

1 (*a*) H. Ishida, ''Handbook of Polybenzoxazine'', H. Ishida, T. Agag, ed. Elsevier, Amsterdam, 2011, Chapter 1, p 1; (*b*) H. Ishida and H. Y. Low, *Macromolecules*, 1997, **30**, 1099; (*c*) H. Ishida and D. J. J. Allen, *J. Polym. Sci., Part B: Polym. Phys.*, 1996, **34**, 1019; (*d*) B. Kiskan, N. N. Ghosh and Y. Yagci, *Polym. Int.*, 2011, **60**, 167; (*e*) L. Jin, T. Agag and H. Ishida, *Eur. Polym. J.*, 2010, **46**, 354.

2 (*a*) C. F. Wang, Y. C. Su, S. W. Kuo, C. F. Huang, Y. C. Sheen and F. C. Chang, *Angew. Chem., Int. Ed.*, 2006, **45**, 2248; (*b*) S. W. Kuo, Y. C. Wu, C. F. Wang and K. U. Jeong, *J. Phys. Chem. C*, 2009, **113**, 20666; (*c*) C. F. Wang, F. C. Chang and S. W. Kuo, *Handbook of Polybenzoxazine*, H. Ishida, T. Agag, ed., Elsevier, Amsterdam, 2011; Chapter 33, p 579.

3 (*a*) S. Rimdusit, S. Pirstpindvong, W. Tanthapanichakoon and S. Damrongsakkul, *Polym. Eng. Sci.*, 2005, **45**, 288; (*b*) T. Agag, A. Akelah, A. Rehab and S. Mostafa, *Polym. Int.*, 2012, **61**, 124.

4 (*a*) D. J. Allen and H. Ishida, *J. Appl. Polym. Sci.*, 2006, **101**, 2798; (*b*) B. Kiskan, B. Aydogan and Y. J. Yagci, *J. Polym. Sci., Part A: Polym. Chem.*, 2009, **47**, 804; (*c*) T. Takeichi, T. Kano, T. Agag, T. Kawauchi and N. J. Furukawa, *J. Polym. Sci., Part A: Polym. Chem.*, 2010, **48**, 5945; (*d*) C. H. Lin, S. L. Chang, T. Y. Shen, Y. S. Shih, H. T. Lin and C. F. Wang, *Polym. Chem.*, 2012, **3**, 935; (*e*) A. D. Baranek, L. L. Kendrick, J. Narayanan, G. E. Tyson, S. Wand and D. L. Patton, *Polym. Chem.*, 2012, **3**, 2892; (*f*) K. C. Chen, H. T. Li, S. C. Huang, W. B. Chen, K. W. Sun and F. C. Chang, *Polym. Int.*, 2011, **60**, 1089; (*g*) K. C. Chen, H. T. Li, W. B. Chen, C. H. Liao, K. W. Sun and F. C. Chang, *Polym. Int.*, 2011, **60**, 436.

5 (*a*) T. Takeichi, Y. Guo and T. J. Agag, *J. Polym. Sci., Part A: Polym. Chem.*, 2000, **38**, 4165; (*b*) T. Takeichi and Y. Guo, *J. Appl. Polym. Sci.*, 2003, **90**, 4075; (*c*) M. Baqar, T. Agag, H. Ishida and S. Qutubuddin, *Polymer*, 2011, **52**, 307; (*d*) J. Jang and D. J. Seo, *J. Appl. Polym. Sci.*, 1998, **67**, 1; (*e*) H. Ardhyananta, M. H. Wahid, M. Sasaki, T. Agag, T. Kawauchi and H. Ismail, *Polymer*, 2008, **49**, 4585.

6 (*a*) S. Tragoonwichian, N. Yanurnet and H. Ishida, *J. Appl. Polym. Sci.*, 2007, **106**, 2925; (*b*) A. Sudo, R. Kudoh, H. Nakayama, K. Arima and T. Endo, *Macromolecules*, 2008, **41**, 9030; (*c*) H. K. Fu, C. F. Huang, S. W. Kuo, H. C. Lin, D. R. Yei and F. C. Chang, *Macromol. Rapid Commun.*, 2008, **29**, 1216; (*d*) C. K. Chozhan, M. Alagar and P. Gnanasundaram, *Acta Mater.*, 2009, **57**, 782; (*e*) Q. Chen, R. W. Xu and D. S. Yu, *Polymer*, 2006, **47**, 7711; (*f*) Y. J. Lee, S. W. Lee, Y. C. Su, J. K. Chen, C. W. Tu and F. C. Chang, *Polymer*, 2004, **45**, 6321; (*g*) Y. J. Lee, J. M. Huang, S. W. Kuo, J. K. Chen and F. C. Chang, *Polymer*, 2005, **46**, 2320; (*h*) Y. J. Lee, S. W. Kuo, C. F. Huang and F. C. Chang, *Polymer*, 2006, **47**, 4378; (*i*) Y. H. Liu and S. X. Zheng, *J. Polym. Sci., Part A: Polym. Chem.*, 2006, **44**, 1168; (*j*) Y. C. Wu and S. W. Kuo, *Polymer*, 2010, **51**, 3948; (*k*) S. W. Kuo and F. C. Chang, *Prog. Polym. Sci.*, 2011, **36**, 1649; (*l*) Q. Chen, R. Xu, J. Zhang and D. Yu, *Macromol. Rapid Commun.*, 2005, **26**, 1878; (*m*) W. H. Hu, K. W. Huang, C. W. Chiou and S. W. Kuo, *Macromolecules*, 2012, **45**, 9020.

7 (*a*) J. M. Huang, S. W. Kuo, Y. J. Lee and F. C. Chang, *J. Polym. Sci., Part B: Polym. Phys.*, 2007, **45**, 644; (*b*) H. Ishida and Y. H. Lee, *Polymer*, 2001, **42**, 6971; (*c*) H. Liu and S. Zheng, *Polymer*, 2003, **44**, 4689; (*d*) H. Ishida and Y. H. Lee, *J. Polym. Sci., Part B: Polym. Phys.*, 2001, **39**, 736; (*e*) J. M. Huang and S. J. Yang, *Polymer*, 2005, **46**, 8068.

8 (*a*) J. M. Dean, N. E. Verghese, H. Q. Pham and F. S. Bates, *Macromolecules*, 2003, **36**, 9267; (*b*) Y. S. Thio, J. Wu and F. S. Bates, *Macromolecules*, 2006, **39**, 7187; (*c*) Z. J. Thompson, M. A. Hillmyer, J. D. Liu, H. J. Sue, M. Dettloff and F. S. Bates, *Macromolecules*, 2009, **42**, 2333; (*d*) J. D. Liu, Z. J. Thompson, H. J. Sue, F. S. Bates, M. A. Hillmyer, M. Dettloff, G. Jocob, N. Verghese and H. Pham, *Macromolecules*, 2010, **43**, 7238.

9 S. Wu, Q. Guo, S. Peng, N. Hameed, M. Kraska, B. Stuhn and Y. W. Mai, *Macromolecules*, 2012, **45**, 3829.

10 (*a*) S. Maiez-Tribut, J. P. Pascault, E. R. Soule, J. Borrajo and R. J. J. Williams, *Macromolecules*, 2007, **40**, 1268; (*b*) Z. Xu

and S. Zheng, *Macromolecules*, 2007, **40**, 2548; (*c*) S. Ritzenthaler, F. Court, I. David, E. Girard-Reydet, I. Leibler and J. P. Pascault, *Macromolecules*, 2002, **35**, 6245; (*d*) F. Meng, Z. Xu and S. Zheng, *Macromolecules*, 2008, **41**, 1411; (*e*) J. Mijovic, M. Shen and J. W. Sy, *Macromolecules*, 2000, **33**, 5235; (*f*) H. Kosonen, J. Ruokolainen, P. Nyholm and O. Ikkala, *Polymer*, 2001, **42**, 9481; (*g*) H. Kosonen, J. Ruokolainen, P. Nyholm and O. Ikkala, *Macromolecules*, 2001, **34**, 3046; (*h*) S. Valkama, A. Nykanen, H. Kosonen, R. Ramani, F. Tuomisto, P. Engelhardt, G. ten Brinke, O. Ikkala and J. Ruokolainen, *Adv. Funct. Mater.*, 2007, **17**, 183; (*i*) J. G. Li and S. W. Kuo, *RSC Adv.*, 2011, **1**, 1822; (*j*) J. G. Li, Y. D. Lin and S. W. Kuo, *Macromolecules*, 2011, **44**, 9295; (*k*) J. G. Li, C. Y. Chung and S. W. Kuo, *J. Mater. Chem.*, 2012, **22**, 18583.

11 (*a*) C. Liang and S. Dai, *J. Am. Chem. Soc.*, 2006, **128**, 5316; (*b*) C. Liang, K. Hong, G. A. Guiochon, J. W. Mays and S. Dai, *Angew. Chem., Int. Ed.*, 2004, **43**, 5785.

12 (*a*) A. Corma, *Chem. Rev.*, 1997, **97**, 2373; (*b*) M. Vallet-Regi, F. Balas and D. Acros, *Angew. Chem., Int. Ed.*, 2007, **46**, 7548; (*c*) J. Zhao, F. Gao, Y. Fu, W. Jin, P. Yang and D. Zhao, *Chem. Commun.*, 2002, 752; (*d*) P. Yang, D. Zhao, D. I. Margolese, B. F. Chmelka and G. D. Stucky, *Chem. Mater.*, 1999, **11**, 2813; (*e*) J. G. Li, T. S. Lee, K. U. Jeong, C. S. Lin and S. W. Kuo, *RSC Adv.*, 2012, **2**, 11242.

13 (*a*) D. Zhao, J. Feng, Q. Huo, N. Melosh, G. H. Fredrickson, B. F. Chmelka and G. D. Stucky, *Science*, 1998, **279**, 548; (*b*) J. G. Li, W. C. Chen and S. W. Kuo, *Microporous Mesoporous Mater.*, 2012, **163**, 34; (*c*) J. G. Li, R. B. Lin and S. W. Kuo, *Macromol. Rapid Commun.*, 2012, **33**, 678.

14 Y. C. Su, W. C. Chen, K. L. Ou and F. C. Chang, *Polymer*, 2005, **46**, 3758.

15 D. Hu and S. Zheng, *Polymer*, 2010, **51**, 6346.

16 Y. C. Su, S. W. Kuo, D. R. Yei, H. Xu and F. C. Chang, *Polymer*, 2003, **44**, 2187.

17 W. H. Hu, K. W. Huang and S. W. Kuo, *Polym. Chem.*, 2012, **3**, 1546.

18 (*a*) S. W. Kuo, S. C. Chan and F. C. Chang, *Polymer*, 2002, **43**, 3653; (*b*) S. W. Kuo, H. C. Lin, W. J. Huang, C. F. Huang and F. C. Chang, *J. Polym. Sci., Part B: Polym. Phys.*, 2006, **44**, 673; (*c*) K. W. Huang, L. W. Tsai and S. W. Kuo, *Polymer*, 2009, **50**, 4876.

19 N. V. Salim, T. Hanley and Q. Guo, *Macromolecules*, 2010, **43**, 7695.

20 (*a*) S. W. Kuo, C. L. Lin and F. C. Chang, *Macromolecules*, 2002, **35**, 278; (*b*) S. W. Kuo, C. F. Huang and F. C. Chang, *J. Polym. Sci., Part B: Polym. Phys.*, 2001, **39**, 1348; (*c*) S. W. Kuo, S. C. Chan and F. C. Chang, *J. Polym. Sci., Part B: Polym. Phys.*, 2004, **42**, 117; (*d*) S. W. Kuo, W. J. Huang, C. F. Huang, S. C. Chan and F. C. Chang, *Macromolecules*, 2004, **37**, 4164; (*e*) S. W. Kuo, W. P. Liu and F. C. Chang, *Macromol. Chem. Phys.*, 2005, **206**, 2307; (*f*) S. W. Kuo, *J. Polym. Res.*, 2008, **15**, 459.

21 (*a*) D. Patterson, *Polym. Eng. Sci.*, 1982, **22**, 64; (*b*) H. Zhang, D. E. Bhagwagar, J. F. Graf, P. C. Paitner and M. M. Coleman, *Polymer*, 1994, **35**, 5379; (*c*) W. H. Jo, Y. K. Kwon and I. H. Kwon, *Macromolecules*, 1991, **24**, 4708; (*d*) S. W. Kuo, S. C. Chan, H. D. Wu and F. C. Chang, *Macromolecules*, 2005, **38**, 4729.

22 S. W. Kuo and F. C. Chang, *Macromol. Chem. Phys.*, 2001, **202**, 3112.

23 S. Jiang, D. Yu, X. Ji, L. An and B. Jiang, *Polymer*, 2000, **41**, 2041.

24 S. Jinag, X. Ji, L. An and B. Jiang, *Polymer*, 2001, **42**, 3901.

25 T. Inoue, *Prog. Polym. Sci.*, 1995, **20**, 119.

26 (*a*) H. L. Chen, S. C. Hsiao, T. L. Lin, K. Yamauchi, H. Hasegawa and T. Hashimoto, *Macromolecules*, 2001, **34**, 671; (*b*) H. L. Chen, J. C. Wu, T. L. Lin and J. S. Lin, *Macromolecules*, 2001, **34**, 6936; (*c*) Y. L. Loo, R. A. Register, A. J. Ryan and G. T. Dee, *Macromolecules*, 2001, **34**, 8968; (*d*) H. L. Chen, S. Y. Lin, Y. Y. Huang, F. C. Chiu, W. Liou and J. S. Lin, *Macromolecules*, 2002, **35**, 9434; (*e*) J. T. Xu, S. C. Turners, J. P. A. Fairclough, S. M. Mai, A. J. Ryan, C. Chaibundit and C. Booth, *Macromolecules*, 2002, **35**, 3614; (*f*) J. Y. Hsu, I. F. Hsieh, B. Nandan, F. C. Chiu, J. H. Chen, U. S. Jeng and H. L. Chen, *Macromolecules*, 2007, **40**, 5014.

27 (*a*) V. Balsamo, F. von Gyldenfeldt and R. Stadler, *Macromolecules*, 1999, **32**, 1226; (*b*) V. Balsamo, F. von Gyldenfeldt and R. Stadler, *Macromol. Chem. Phys.*, 1996, **197**, 3317; (*c*) W. C. Chen, S. W. Kuo, C. H. Lu and F. C. Chang, *Macromolecules*, 2009, **42**, 3580; (*d*) I. H. Lin, S. W. Kuo and F. C. Chang, *Polymer*, 2009, **50**, 5276; (*e*) W. C. Chen, S. W. Kuo and F. C. Chang, *Polymer*, 2010, **51**, 4176.

28 (*a*) W. Fan, L. Wang and S. Zheng, *Macromolecules*, 2009, **42**, 327; (*b*) D. Hu, Z. Xu, K. Zeng and S. Zheng, *Macromolecules*, 2010, **43**, 2960.

29 H. Kosonen, S. Valkama, A. Nykanen, M. Toivanen, G. ten Brinke, J. Ruokolainen and O. Ikkala, *Adv. Mater.*, 2006, **18**, 201.

30 W. D. Harkin and G. Jura, *J. Am. Chem. Soc.*, 1944, **66**, 1366.

31 O. Becker, Y. B. Cheng, R. J. Varley and G. P. Simon, *Macromolecules*, 2003, **36**, 1616.

32 J. G. Li, Y. H. Chang, Y. S. Lin and S. W. Kuo, *RSC Adv.*, 2012, **2**, 12973.

